Improved Model Predictive Control with Prescribed Performance for Aggregated Thermostatically Controlled Loads

Yang Yu, Li Quan, Zengqiang Mi, Jianbin Lu, Shengqiang Chang, and Yubao Yuan

***Abstract*—Aggregate thermostatically controlled loads (ATCLs) are a suitable candidate for power imbalance on demand side to smooth the power fluctuation of renewable energy. A new control scheme based on an improved bilinear aggregate model of ATCLs is investigated to suppress power imbalance. Firstly, the original bilinear aggregate model of ATCLs is extended by the second-order equivalent thermal parameter model to optimize accumulative error over a long time scale. Then, to ensure the control performance of tracking error, an improved model predictive control algorithm is proposed by integrating the Lyapunov function with the error transformation, and theoretical stability of the proposed control algorithm is proven. Finally, the simulation results demonstrate that the accuracy of the improved bilinear aggregate model is enhanced; the proposed control algorithm has faster convergence speed and better tracking accuracy in contrast with the Lyapunov function-based model predictive control without the prescribed performance.**

***Index Terms*—Lyapunov function, model predictive control, power tracking, prescribed performance, thermostatically controlled load.**

I. Introduction

THE bulk of intermittent renewable energy integrated with the power grid triggers the power imbalance between the supply side and demand side [1]. The common way to solve the power imbalance is to use power plants such as thermal power plants to provide ancillary services on the supply side. It reduces the operating efficiency of the system with plenty of spare capacity required [2]. Alternatively, the emergence of energy storage technologies that could be employed in different locations of the power system is an outstanding solution for power imbalance but lies in relatively high cost [3]. Recent studies have revealed that a large aggregation of thermostatically controlled loads (TCLs) such as air conditioners and electric water heaters on the demand side offer an ideal option for ancillary services with the advantages of large capacity and fast response [4], [5]. However, the fundamental challenge faced in the dispatch of large-scale and widely distributed TCLs lies in the modeling and control of TCLs [6].

One of the key issues in the challenge is to establish an accurate model to describe the dynamic evolutionary behavior of aggregate thermostatically controlled loads (ATCLs) over a time scale as long as possible. The modeling of ATCLs currently includes four methods: state-space equation [7], state sequence [8], Fokker-Planck equation [9], and bilinear equations [10]. Among them, the bilinear model built by bilinear equations has high accuracy and can be easily applied for control. It uses the finite difference to discretize an actual temperature range into several limited temperature intervals. TCLs in the bilinear model are distributed in these temperature intervals. Through changing the set-point temperature, TCLs will be redistributed among these temperature intervals to output the required power. The accuracy of the bilinear model also depends on the model of individual TCL, where most of the literature adopts the first-order equivalent thermal parameter (ETP) model to simulate the dynamic thermal behavior of buildings and the indoor mass temperature is ignored [11]-[14]. The first-order ETP model is not accurate enough for disregarding the coupling effect between indoor mass temperature and indoor air temperature. Previous research work [15] on population dynamics of TCLs has demonstrated that the second-order ETP model is more accurate with consideration of the coupling effect. But current studies on modeling the ATCLs through the second-order ETP model primarily use the average transfer rates to replace the real transfer rates, which leads to an imprecise model over a long time scale.

Another further problem is to study the control algorithm based on the aggregate model of ATCLs. Through changing the set-point temperature of ATCLs in [16], the signal from automatic generation control is tracked well by ATCLs. Hierarchical control of ATCLs is designed in [17] for primary frequency support. A group control based model predictive

Manuscript received: November 30, 2020; revised: March 15, 2021; accepted: May 13, 2021. Date of CrossCheck: May 13, 2021. Date of online publication: June 11, 2021.

This work was supported by the key projects in 2018 National Key R&D Programs (No. 2018YFE0122200), the Fundamental Research Funds for the Central Universities (No. 2020MS090), and opening project of Hebei Smart Grid Distribution and Utilization Technology Innovation Center (No. 20200803).

Y. Yu (corresponding author), L. Quan, Z. Mi, and J. Lu are with the State Key Laboratory of Alternate Electrical Power System with Renewable Energy Sources, North China Electric Power University, Baoding, China (e-mail: yym0401@163. com; 1057863783@qq. com; mizengqiang@sina. com; lujianbin_l@163.com).

S. Chang and Y. Yuan are with the Innovation Center for Hebei Intelligent Grid Distribution Technology, Shijiazhuang Kelin Electric Co., Ltd., Shijiazhuang, China (e-mail: ql817516@163.com; ql1057863783@163.com).

DOI: 10.35833/MPCE.2020.000834

control (MPC) scheme is proposed in [18] for ATCLs to participate in demand response. An MPC framework used for the aggregation of air conditioners is developed in [19] to compensate for the fluctuation of photovoltaic power. The above argument shows that MPC is widely used in the field of ATCLs due to its strong robustness and high accuracy [20]. However, the traditional MPC is optimized repeatedly in every sampling point and requires massive computation, which delays the execution time to some extent [21]. Besides, little attention has been paid to prescribed performance control (PPC). It is hard and even unknown for current control approaches of ATCLs to estimate the control effect without prescribed performance. Until now, PPC has been extensively applied to several control areas [22]-[24]. A neural adaptive output tracking PPC of a chaotic permanent magnet synchronous motor system is investigated in [25], and adaptive control with prescribed performance for active suspension systems is designed in [26].

In this paper, for the first issue of aggregate modeling, the bilinear aggregate model (BAM) of ATCLs is firstly extended in terms of the second-order ETP model with average load transfer rates. But the extended model called SBAM fits only a small change of set-point temperature. To further enhance the accuracy of modeling over a longer time scale, an improved SBAM (ISBAM) is built taking into account the real indoor mass temperature and set-point temperature. For another issue of the control approach, an improved Lyapunov function-based MPC (ILMPC) algorithm with prescribed performance is proposed. The simulation results show that the ISBAM is more accurate than the ordinary aggregate model. The proposed ILMPC algorithm reduces the computation time and confines tracking performance within a prescribed boundary as compared with traditional MPC.

The contributions of this paper are manifested as follows: ① by considering the indoor mass temperature, the original BAM of ATCLs is improved to build a more accurate ISBAM; ② a Lyapunov function-based MPC algorithm with prescribed performance is presented for ATCLs to less execution time while ensuring control performance both in steady state and transient state.

The remainder of this paper is organized as follows. Section II derives the ISBAM for ATCLs. The ILMPC approach is developed in Section III. The simulation is conducted in Section IV to verify the precision of the improved model and the effectiveness of the proposed control approach. Section V draws out some conclusions.

II. SYSTEM MODELING

A. Dynamic Thermal Model of Individual TCL

The disregarding of the coupling effect between indoor mass temperature and indoor air temperature in the first-order ETP model results in the fact that it cannot accurately describe the real dynamic thermal behavior of TCL in transient response such as the change of set-point temperature. A second-order ETP model [27] is used to depict the dynamic thermal process of individual TCL, which selects indoor mass temperature and indoor air temperature as two state variables. It calls a two-mass model and its differential equation is expressed as:

$$\begin{cases} \dot{T}_a(t) = -\left(\dfrac{1}{R_m C_a} + \dfrac{1}{R_a C_a}\right) T_a(t) + \dfrac{1}{R_m C_a} T_m(t) + \\ \qquad \dfrac{1}{R_a C_a} T_\infty(t) - m(t) \dfrac{1}{C_a} P(t) \\ \dot{T}_m(t) = \dfrac{1}{R_m C_m}\big(T_a(t) - T_m(t)\big) \\ m(t) = \begin{cases} 0 & T_a(t) \le T_{\min} \\ 1 & T_a(t) \ge T_{\max} \\ m(t-\Delta t) & \text{others} \end{cases} \\ T_{\min} = T_{set} - \dfrac{\delta_{db}}{2} \\ T_{\max} = T_{set} + \dfrac{\delta_{db}}{2} \end{cases} \tag{1}$$

where $T_a(t)$ is the indoor air temperature; $T_m(t)$ is the indoor mass temperature; $T_\infty(t)$ is the outdoor ambient temperature; P is the operating power of an individual TCL; $T_{\max}$ and $T_{\min}$ are the upper and lower limits of temperature, respectively; T_{set} is the set-point temperature; δ_{db} is the temperature deadband; C_a is the heat capacity of indoor air; R_a is the indoor air thermal resistance; C_m is the heat capacity of the indoor mass; R_m is the indoor mass thermal resistance; t is the time; $m(t)$ is the switching variable; and Δt is the time step.

The corresponding dynamic thermal equivalent circuit of the two-mass model is shown in Fig. 1, where $R_a = 1/Q_a$, $R_m = 1/Q_m$, Q_a and Q_m are the heat loss coefficients of indoor air and indoor mass, respectively.

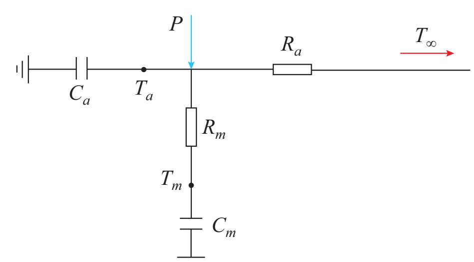

Fig. 1. Thermal equivalent circuit of second-order ETP model for individual TCL.

The aggregate power P_r based on the second-order ETP model is:

$$P_r(t) = \sum_{i=1}^{N} \frac{1}{\eta_i} m_i(t) P(t) \tag{2}$$

where η_i is the efficiency of the i^{th} TCL; and N is the number of TCLs.

B. Improved Bilinear Aggregate Model of ATCLs

1) Bilinear Aggregate Model Based on Second-order ETP Model

Both the continuous temperature variable and "ON/OFF" discrete variable included in the second-order ETP model of TCL make it complex to use for control design, even though the model can precisely represent its power consumption. If each TCL is expressed as an independent ETP model, the aggregate model describing a huge number of TCLs will inevitably confront the disaster of dimensionality.

Control-oriented original BAM of ATCLs constructed through the first-order ETP model in [28] is extended in the research by the second-order ETP model to establish the SBAM, which is written in (3). It is assumed that all TCLs in the model are distributed in a finite temperature range [T_l, T_h], and the temperature range is cut into several small and equal intervals. TCLs with two states of "ON/OFF" are contained in each interval.

$$\begin{cases} \dot{\boldsymbol{X}}(t)=\boldsymbol{AX}(t)+\boldsymbol{BX}(t)u(t) \\ P_T(t)=\boldsymbol{CX}(t) \end{cases} \tag{3}$$

where $\boldsymbol{X}(t)=\left[x_1(t), x_2(t), \ldots, x_L(t)\right]^{\mathrm{T}}$ is an $L\times 1$ state variable matrix representing the number of TCLs in each temperature interval after the finite difference discretization, L is the number of temperature intervals; $u(t)=\dot{T}_{set}(t)$ is the control input; $P_T(t)$ is the total consuming power of ATCLs; $\boldsymbol{C}=\left[\underbrace{0,\ldots,0}_{L/2}, \underbrace{P,\ldots,P}_{L/2}\right]\Big/\eta_i$ is an $L\times 1$ output matrix; $\boldsymbol{A}=\boldsymbol{A}\left(\alpha_{on}, \alpha_{off}\right)$ is an $L\times L$ matrix; and $\boldsymbol{B}$ is also an $L\times L$ matrix with the same structure as matrix $\boldsymbol{A}$. Please see matrix $\boldsymbol{A}$ in Appendix A for details, where α_{on} and α_{off} in matrix $\boldsymbol{A}$ are the load transfer rates of TCL over the ON and OFF states, respectively, which can be calculated by (4). α_{on} and α_{off} in matrix $\boldsymbol{A}$ are set to be -1 to obtain matrix $\boldsymbol{B}$, i.e., $\boldsymbol{B}=\boldsymbol{A}(-1,-1)$.

$$\begin{cases} \alpha_{on}=-\left(\dfrac{1}{R_mC_a}+\dfrac{1}{R_aC_a}\right)T_a(t)+\dfrac{T_m(t)}{R_mC_a}+\dfrac{T_\infty}{R_aC_a}-\dfrac{P}{C_a} \\ \alpha_{off}=-\left(\dfrac{1}{R_mC_a}+\dfrac{1}{R_aC_a}\right)T_a(t)+\dfrac{T_m(t)}{R_mC_a}+\dfrac{T_\infty}{R_aC_a} \end{cases} \tag{4}$$

To reduce the amount of computation, the load transfer rates $\alpha_{on/off}$ in each temperature interval are approximated in the average transfer rates $\bar{\alpha}_{on/off}$ under the expected set-point temperature T_{set}^{des} and the initial indoor mass temperature T_{m0}. Then, $\boldsymbol{A}$ becomes a constant matrix $\boldsymbol{A}\left(\bar{\alpha}_{on}, \bar{\alpha}_{off}\right)$, and (4) could be simplified and written as:

$$\begin{cases} \bar{\alpha}_{on}=-\left(\dfrac{1}{R_mC_a}+\dfrac{1}{R_aC_a}\right)T_{set}^{des}+\dfrac{T_{m0}}{R_mC_a}+\dfrac{T_\infty}{R_aC_a}-\dfrac{P}{C_a} \\ \bar{\alpha}_{off}=-\left(\dfrac{1}{R_mC_a}+\dfrac{1}{R_aC_a}\right)T_{set}^{des}+\dfrac{T_{m0}}{R_mC_a}+\dfrac{T_\infty}{R_aC_a} \end{cases} \tag{5}$$

2) Improved Bilinear Aggregate Model Based on Second-order ETP Model

The SBAM only suits for a relatively small variation of the set-point temperature T_{set}. When T_{set} deviates greatly from its expected value T_{set}^{des}, if the average transfer rates $\bar{\alpha}_{on/off}$ are still used to express the real transfer rates $\alpha_{on/off}$, the SBAM will be inaccurate over a long time scale and the comparative results will be demonstrated in Section IV.

Hence, the real mass temperature $T_m(t)$ and real set-point temperature $T_{set}(t)$ are used to express the transfer rates $\alpha_{on/off}$. A new group of transfer rates $\hat{\alpha}_{on/off}$ can be written as:

$$\begin{cases} \hat{\alpha}_{on}=\bar{\alpha}_{on}-\left(\dfrac{1}{R_mC_a}+\dfrac{1}{R_aC_a}\right)\Delta T_{set}(t)+\dfrac{\Delta T_m(t)}{R_mC_a} \\ \hat{\alpha}_{off}=\bar{\alpha}_{off}-\left(\dfrac{1}{R_mC_a}+\dfrac{1}{R_aC_a}\right)\Delta T_{set}(t)+\dfrac{\Delta T_m(t)}{R_mC_a} \end{cases} \tag{6}$$

Thus, the ISBAM based on $\hat{\alpha}_{on/off}$ can be derived as:

$$\begin{cases} \dot{\boldsymbol{X}}(t)=\boldsymbol{AX}(t)+\boldsymbol{BX}(t)U(t) \\ U(t)=u_1(t)+\left(\dfrac{1}{R_mC_a}+\dfrac{1}{R_aC_a}\right)u_2(t)-\dfrac{1}{R_mC_a}u_3(t) \\ P_T(t)=\boldsymbol{CX}(t) \end{cases} \tag{7}$$

where $u_1(t)$ and $u_2(t)$ reflect the real-time and cumulative effects with the change of set-point temperature on the evolutionary process of ATCLs, respectively; and $u_3(t)$ indicates the influence of the two-mass model. The matrices $\boldsymbol{A}$ and $\boldsymbol{B}$ remain unchanged and are still constant matrices. $u_1(t)=\dot{T}_{set}(t)$, $u_2(t)=\Delta T_{set}=T_{set}(t)-T_{set}^{des}$, and $u_3(t)=\Delta T_m=\dot{T}_m(t)-T_{m0}$. As the indoor mass temperature $T_m(t)$ is not easy to obtain, its estimation $\hat{T}_m(t)$ is used instead, given by:

$$\dot{\hat{T}}_m(t)=\frac{1}{R_mC_m}\left(T_{set}(t)-\hat{T}_m(t)\right) \tag{8}$$

Equation (9) can be obtained by discretizing (8), and the estimated value of indoor mass temperature $T_m(t)$ could be obtained by continuous iteration through (9).

$$T_m(k+1)=dT_m(k)+(1-d)\,T_{set}(k) \tag{9}$$

where $d=\mathrm{e}^{-\frac{1}{R_mC_m}\Delta t}$.

The dynamic process of TCLs after finite-difference discretization is shown in Fig. 2, where ΔT is the discrete temperature length; x_1-x_{10} are the numbers of TCL loads at "OFF" state; and x_{11}-x_{20} are the numbers of TCL loads at "ON" state. We can see that the change in the number of TCL obeys a certain rule. By controlling T_{set}, the flow of TCLs between the adjacent temperature intervals can be changed, which is similar to the direct control of TCL to achieve the regulation of aggregate power.

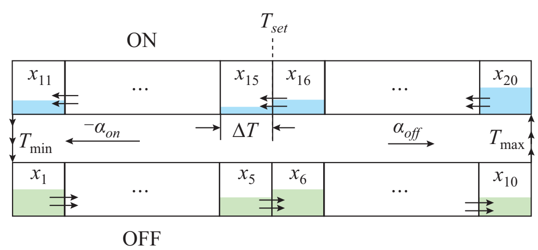

Fig. 2. Dynamic process of TCLs after finite-difference discretization.

III. Controller Design

A. Description of Control Problem

The control goal is to devise an ILMPC algorithm with prescribed performance for the ISBAM to track a given reference trajectory. The major difference between the modified MPC and traditional MPC is that the optimal control law in the modified MPC is directly determined through a constructed Lyapunov function, which guarantees the stability and reduces the computational burden. Hence, minimizing the cost function to obtain the control signal in traditional MPC is avoided. Moreover, in combination with the prescribed performance function (PPF), the tracking error can be assumed to converge to a predefined arbitrarily small residual set both in steady state and transient state [29]-[31]. The control flow chart is shown in Fig. 3, where $e_y(t)$ is the tracking error, $e_y(t) = P_T(t) - P_{ref}(t)$; and P_{ref} is the reference power.

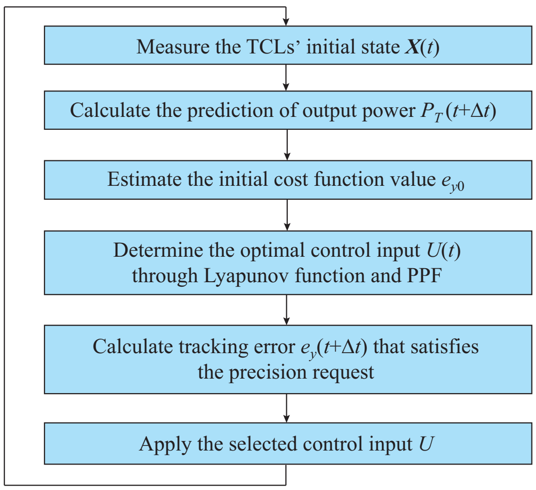

Fig. 3. Control flow chart of ILMPC.

B. Tracking Error Transformation

Lemma 1: considering a dynamic system $\dot{x} = f(x,t)$, for a given bounded initial conditions, if there exists a continuous and positive Lyapunov function $V(x)$ satisfying $\dot{V}(x) \le -\eta_a V(x) + \gamma$, where η_a and γ are positive constants, then the solution $x(t)$ of the system is semi-global uniformly ultimate bounded.

Proof: please refer to [32] for detailed derivation.

In terms of the elaborately designed PPF [33], the tracking error $e_y(t)$ could be constrained as:

$$-\delta_1 \rho(t) < e_y(t) < \delta_2 \rho(t) \tag{10}$$

where δ_1 and δ_2 are the positive design parameters; and $-\delta_1 \rho(0) < e_{y0} < \delta_2 \rho(0)$, where $e_{y0} = e_y(0)$; $\rho(t)$ is a bounded, smooth, strictly positive, and decreasing function used to specify the error boundary range called performance function, and it can be designed as:

$$\rho(t) = \left(\rho_0 - \rho_\infty\right) \mathrm{e}^{-rt} + \rho_\infty \tag{11}$$

where $\rho_0 = \rho(0)$, and ρ_0 is selected such that $\rho_0 > \rho_\infty$; ρ_∞ represents the maximum allowable boundary of $e_y(t)$ in the steady state that can be set as an arbitrarily small value to ensure the practical convergence of $e_y(t)$ to be zero. Moreover, the rate of convergence for $\rho(t)$ is related to the constant r.

In contrast with the other conventional prescribed performance functions like preset time performance function given in (12), Fig. 4 shows that the exponential prescribed performance function shown in (11) has a faster convergence speed with the same initial control parameters $\rho_0 = 100$ and $\rho_\infty = 0.4$, where the other parameters of the two performance functions are chosen reasonably as $r = 0.5$, $T_z = 50$ s, and $h = 5$. Hence, the exponential prescribed performance function is employed to constrain $e_y(t)$.

$$\rho(t) = \left(\rho_0 - \rho_\infty\right)\left(1 - \frac{t}{T_z}\right)^h + \rho_\infty \tag{12}$$

where T_z is the preset convergence time; and h is a positive constant larger than 2.

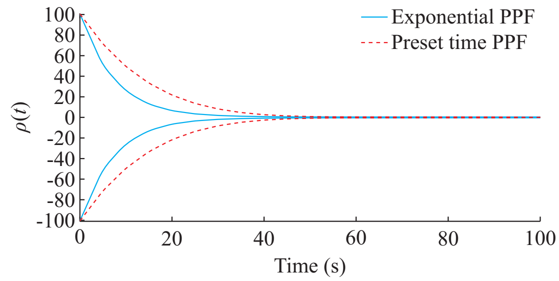

Fig. 4. Simulation results for exponential PPF and preset time PPF.

To achieve the control performance depicted in (10) more conveniently, an equivalent unconstraint condition is built as:

$$s(t) = \phi\left(\frac{e_y(t)}{\rho(t)}\right) \tag{13}$$

where s is known as the transformation error; and ϕ is the smooth and strictly increasing function satisfying (14):

$$\phi: \left(-\delta_1, \delta_2\right) \to \left(-\infty, +\infty\right) \tag{14}$$

According to (13), the transformation error s could be represented as:

$$s = \frac{1}{2}\left(\ln\left(\delta_1\delta_2 + v_1\delta_2\right) - \ln\left(\delta_1\delta_2 - v_1\delta_1\right)\right) \tag{15}$$

Its first derivative is:

$$\dot{s} = \xi\left(\dot{e}_y - e_y\frac{\dot{\rho}}{\rho}\right) \tag{16}$$

where $\xi = \dfrac{1}{2\rho}\left(\dfrac{1}{\delta_1 + v_1} - \dfrac{1}{v_1 - \delta_2}\right) > 0$; and $v_1 = \dfrac{e_y}{\rho}$.

Lemma 2: for the tracking error signal $e_y(t)$ and corresponding transformation error $s(t)$ defined by (13) and satisfying (14), if $s(t)$ is bounded, $e_y(t)$ will satisfy (10) for all $t \ge 0$.

Proof: we assume that there exist two unknown constants s_1 and s_2 such that:

$$s_1 < s(t) < s_2 \tag{17}$$

By using the inverse transformation ϕ^{-1} for all $t \ge 0$, (13) could be written as:

$$\phi^{-1}\left(s_1\right)\rho(t) < e_y(t) < \phi^{-1}\left(s_2\right)\rho(t) \quad \forall t \ge 0 \tag{18}$$

Finally, in terms of (14), we can obtain:

$$-\delta_1 \rho(t) < e_y(t) < \delta_2 \rho(t) \tag{19}$$

Hence, Lemma 2 holds.

Lemma 3: for any $x \in \mathbf{R}$ and arbitrary constant $\varepsilon > 0$, the following inequality (20) holds.

$$0 \le |x| \le \varepsilon + \frac{x^2}{\sqrt{x^2+\varepsilon^2}} \tag{20}$$

Proof: please refer to [34] for detailed derivation.

C. Design of Lyapunov Function-based MPC with Prescribed Performance

This section is to design the ILMPC algorithm.

Step 1: (7) is chosen as the prediction model and rewritten as:

$$\begin{cases} \dot{\boldsymbol{X}}(t) = \boldsymbol{AX}(t) + \boldsymbol{BX}(t)U(t) \\ P_T(t) = \boldsymbol{CX}(t) \end{cases} \tag{21}$$

Step 2: the transformation error is rewritten in accordance with (16) and (21) and shown as:

$$\dot{s} = \xi\left(\boldsymbol{CAX} + \boldsymbol{CBX}U - \dot{P}_{ref} - e_y\frac{\dot{\rho}}{\rho}\right) \tag{22}$$

The Lyapunov function of the system is defined as $V = \frac{1}{2}s^2$. Then, we can obtain:

$$\dot{V} = s\xi\left(\boldsymbol{CAX} + \boldsymbol{CBX}U - \dot{P}_{ref} - e_y\frac{\dot{\rho}}{\rho}\right) \tag{23}$$

According to the Lyapunov stability theory and prescribed performance control, the optimal control law is designed as:

$$U = -\frac{s\alpha^2}{\boldsymbol{CBX}\xi\sqrt{s^2\alpha^2+\varepsilon^2}} \tag{24}$$

where $\alpha = \xi\boldsymbol{CAX} - \xi\dot{P}_{ref} - \xi e_y\frac{\dot{\rho}}{\rho} + k_1 s$.

In terms of Lemma 3, the expression of $s\xi\boldsymbol{CX}U$ could be written as:

$$s\xi\boldsymbol{CX}U \le |s\xi\boldsymbol{CBX}U| \le \varepsilon - s\alpha \tag{25}$$

where $\varepsilon > 0$.

Substituting (25) into (23), we can obtain:

$$\dot{V} \le -k_1 s^2 + \varepsilon = -\eta V + \varepsilon \tag{26}$$

It follows from (26) that:

$$V \le \left(V(0) - \frac{\varepsilon}{\eta}\right)\mathrm{e}^{-\eta t} + \frac{\varepsilon}{\eta} \tag{27}$$

By Lemma 1, $V(s)$ is bounded and exponentially convergent in (27), which shows that s is bounded. By Lemma 2 and the appropriate choices of the performance function $\rho(t)$ and the constants δ_1 and δ_2, the tracking error $e_y(t)$ could remain within the prescribed performance boundary when $t \ge 0$.

Theorem 1: Considering the system (21) and the controller (24), the closed-loop system is stable and the tracking error converges to a neighborhood of the origin within the prescribed performance boundary for all $t \ge 0$.

IV. Simulation Study

A. Accuracy Analysis of ISBAM

For evaluating the accuracy of ISBAM, 1000 TCLs are chosen to analyze the performance of the first-order ETP model, second-order ETP model, SBAM, and ISBAM through the Monte Carlo simulation method. In order to make the selected parameters of TCLs closer to the actual situation and ensure the parameters of TCLs to be non-uniform, the parameters of TCLs are taken as a series of log-normally distributed functions with the expected values of the distributed functions as shown in Table I, where the parameter C is the thermal capacitance; and T_{set0}^{des} is the initial expected set-point temperature. The standard deviations of the normally distributed functions are set to be 0.2. The initial state is placed at 42.8% of the TCL load in the ON state. The results are presented in Figs. 5 and 6.

TABLE I
TYPICAL PARAMETERS OF INDIVIDUAL TCL

Parameter	Value	Parameter	Value
R_a (°C/kW)	2	η	2
R_m (°C/kW)	1	T_{set0}^{des} (°C)	25
C (kWh/°C)	10	P (kW)	12
C_a (kWh/°C)	0.75C	T_{m0} (°C)	24
C_m (kWh/°C)	0.25C	T_∞ (°C)	35
δ_{db} (°C)	1	L	200

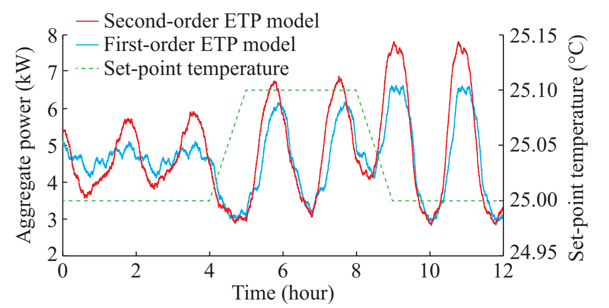

Fig. 5. Comparative results of first-order ETP model with second-order ETP model.

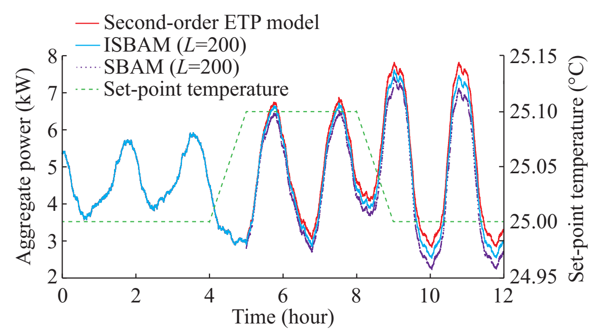

Fig. 6. Comparative results among second-order ETP model, SBAM, and ISBAM.

Figure 5 indicates that the second-order ETP model has a longer period and larger amplitude of power fluctuation in comparison to the first-order ETP model when the set-point temperature is changed. The reason is that, compared with the first-order ETP model that only considers the indoor air temperature, the second-order ETP model considers more about the nature of the heat capacity and thermal resistance embodied in the indoor mass, making it have a longer power fluctuation period and larger fluctuation amplitude when the set-point temperature is changed. The second-order ETP model better reflects the real operation situation of TCL.

In Fig. 6, the cumulative error of SBAM is further improved by ISBAM over a long time scale. Hence, ISBAM is more accurate than SBAM in describing the power evolutionary process of ATCLs.

B. Simulation Analysis of Proposed Control Approach

To illustrate the validity of the presented ILMPC with prescribed performance, a three-layer control architecture is presented in Fig. 7, which includes synchronous generators, renewable energy, and one TCL aggregator with a total of 10000 TCLs. WP stands for wind power and PV stands for photovoltaic. The dispatch plan is first released by the dispatch center at the upper level. The TCL aggregator at the intermediate level will receive the given reference power. At the lower level, 10000 TCLs are aggregated to participate in ancillary services by ILMPC approach.

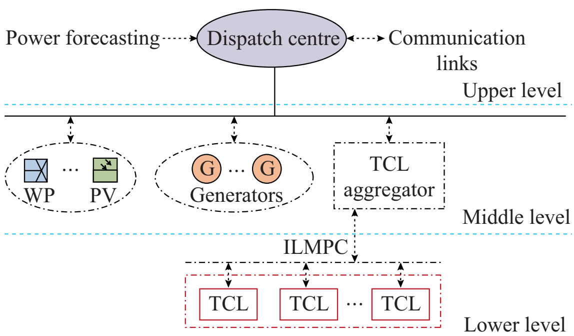

Fig. 7. Schematic diagram of example system.

About the selection of parameters, it is known that δ_1 and δ_2 are usually taken as 1; r, ρ_0, and ρ_∞ can be selected according to the initial state of the controlled system and the desired preset performance. Generally, we use $-\delta_1\rho(0)<e_{y0}<\delta_2\rho(0)$ to determine ρ_0; r is larger than zero, and ρ_∞ is a positive number close to zero. For practical application scenarios, the optimal control parameters can be identified based on the trial-and-error method and previous experience.

To verify the control performance better, the comparative analysis with the Lyapunov function-based MPC (LMPC) algorithm without prescribed performance is investigated and three cases are conducted.

1) Case 1: Tracking Constant Power

The objective is to regulate ATCLs to provide 40 MW power in 30 minutes. Six initial conditions of e_{y0} are 0.0175, 0.0451, 0.0947, −0.0239, −0.0515 and −0.0929, respectively. The design parameters of the controller and PPF are chosen as $\rho_0=0.1009$, $\delta_1=1$, $\delta_2=1$, $r=0.9$, and $\rho_\infty=0.009$. The simulation results are given in Figs. 8-10. Figure 8 shows that the proposed control algorithm is superior to the comparative algorithm that fails to regulate the tracking error to be within the PPF bound. The proposed control algorithm also has a faster transient convergence speed and satisfies the performance constraint in various initial states.

Moreover, Fig. 8 also shows that the power tracking error takes some time to be stabilized. The fact is that the change rate of the set-point temperature is less than the rate of load flow over the temperature interval to ensure the stability of the bilinear aggregate model, which makes the load change of the aggregate model reflect a slow evolutionary process.

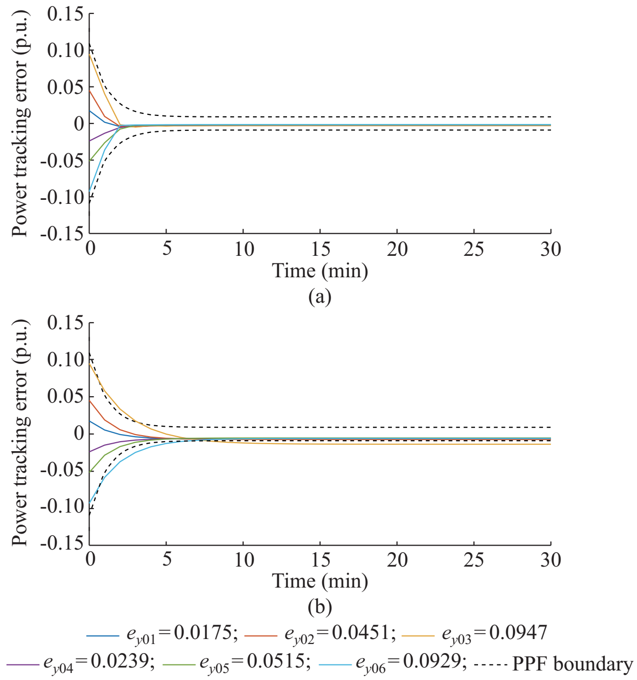

Fig. 8. Comparison of power tracking error with different control approaches. (a) Proposed ILMPC. (b) LMPC without prescribed performance.

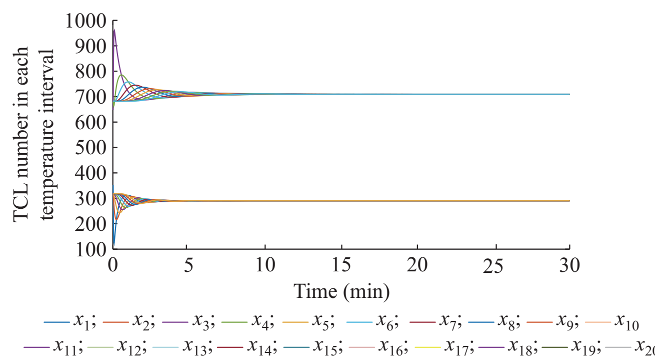

Fig. 9. Change in number of TCLs in each temperature interval.

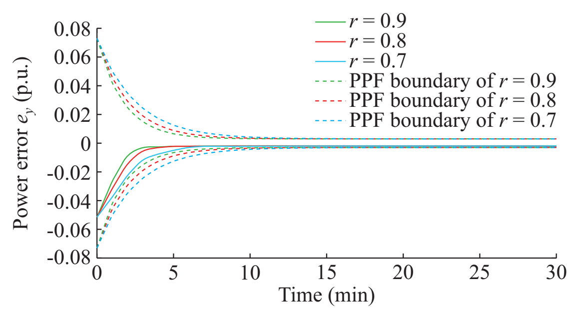

Fig. 10. Power errors e_y with different r.

For the initial state $e_{y0}=0.0451$ and the reference power $P_{ref}=40$ MW, with the aid of the proposed control algorithm, we observe the change in the number of TCLs. The result is shown in Fig. 9. There are 20 temperature intervals, including 10 temperature intervals at ON state and 10 temperature intervals at OFF state. We can observe that there are 20 curves and each curve represents the number of TCLs in the corresponding temperature interval. In the power tracking process, the number of TCLs in each temperature interval changes constantly and finally reaches a balance, but it is a slow evolutionary process and cannot be completed quickly.

Figure 10 shows the convergence of power errors with different r, which indicates the decreasing rate of PPF. We observe that the larger r is, the faster the error convergence speed will be. But it should be pointed out that r cannot be selected too large. Otherwise, the result is likely to diverge.

2) Case 2: Tracking Variable Power

We will further validate the improved performance of the proposed PPF-based ILMPC control scheme. In this case, a more realistic reference power $P_{ref}=40+0.3\sin(\pi t/3)$ MW is used in the first group simulation. The initial tracking error $e_{y0}=-0.0515$ and the design parameters of the controller and PPF are chosen as $\rho_0=0.05$, $\delta_1=1$, $\delta_2=1$, $r=0.8$, and $\rho_\infty=0.006$. The simulation results are shown in Fig. 11(a) and (b). In the second group simulation, we increase the fluctuation amplitude of the reference power that is $P_{ref}=40+0.6\sin(\pi t/3)$ MW. The initial tracking error $e_{y0}=0.0451$ and the design parameters of the controller and PPF are chosen as $\rho_0=0.05$, $\delta_1=1$, $\delta_2=1$, $r=0.8$, and $\rho_\infty=0.01$. The simulation results are shown in Fig. 11(c) and (d). Figure 11 shows that the proposed PPF-based control can provide better tracking performance for fluctuating reference power and e_y can be retained within the PPF bound compared with the LMPC scheme without prescribed performance of $e_y(t)$ under the same initial condition.

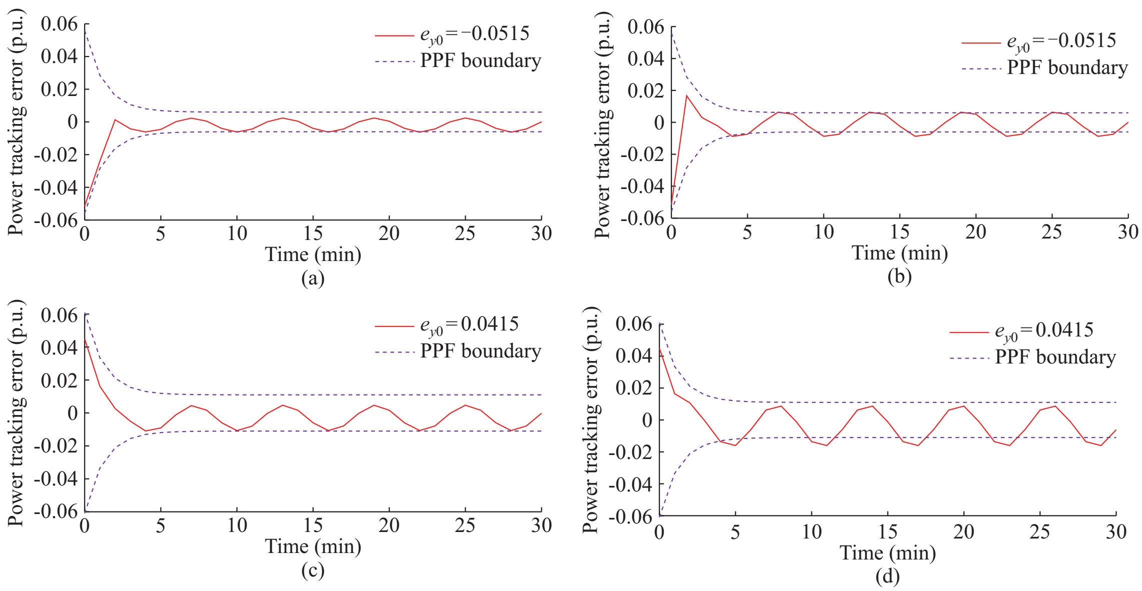

Fig. 11. Comparisons of power tracking error with different control approaches under more realistic reference power. (a) Proposed ILMPC in the first group simulation. (b) LMPC in the first group simulation. (c) Proposed ILMPC in the second group simulation. (d) LMPC in the second group simulation.

For practical applications, TCL parameters on the load side may be different, and there will also be uncertainties on the generation side. The control effect of ATCLs may be affected by the change of TCL parameters. The controller must be robust enough to make sure that the reference signal can be accurately tracked under external disturbances. In order to further verify the robustness of the proposed control algorithm, when the TCL parameters change in the range of –40%-40%, the tracking effect of the proposed algorithm and LMPC algorithm is compared and simulated, and the results are shown in Fig. 12. The reference power is $P_{ref}=40+0.2\sin(\pi t/3)$ MW. The initial tracking error is $e_{y0}=0.0451$ and the design parameters of the controller and PPF are chosen as $\rho_0=0.05$, $\delta_1=1$, $\delta_2=1$, $r=0.7$, and $\rho_\infty=0.007$.

Figure 12 shows the performance of the proposed ILMPC and LMPC when the model parameters vary from –40% to 40%. The variations of these parameters have a slight impact on the control performance for the proposed ILMPC, which guarantees the tracking power error within the PPF bound and ensures the robustness of the proposed control algorithm. However, the LMPC without prescribed performance cannot guarantee the tracking power error within the PPF boundary with parameter variations.

3) Case 3: Suppression of Power Fluctuation of Renewable Energy

The consuming power of ATCLs is used to smooth the power fluctuation of renewable energy. The desired trajectory P_{ref} of ATCLs is delivered by the dispatch center. The generation power data and load power data of the system within two hours are shown in Fig. 13, which shows that the load power is greater than the generation power in the previous one hour, owing to the large demand for the rigid load. Thus, it is feasible to reduce ATCLs to achieve the power balance between supply side and demand side. In the next hour, the generation power is greater than the load power with the unexpected increase of renewable power output.

Due to the suddenness and randomness of renewable power output, it is difficult to meet the load demand by only adjusting the conventional generators, which is restricted by climbing rates and the minimum technical outputs. By regulating ATCLs to consume the surplus power of renewable energy, the power imbalance will be effectively alleviated and the curtailment of WP or PV power will also be prevented.

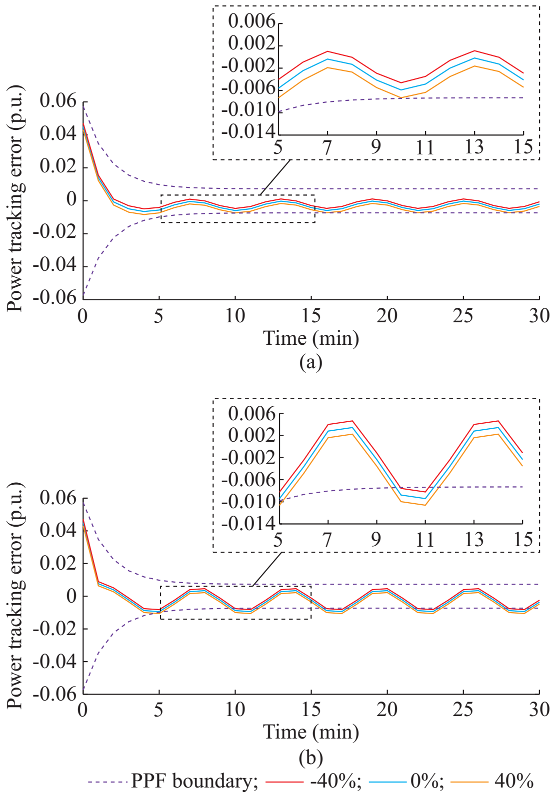

Fig. 12. Robustness analysis with uncertainties in the model parameters. (a) Proposed ILMPC. (b) LMPC without prescribed performance.

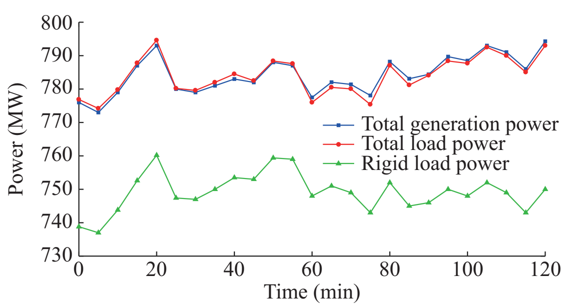

Fig. 13. Power generation and consumption of system.

To track the given reference trajectory P_{ref}, the largest value among the initial conditions is $e_{y0}=-0.0757$ that satisfies the inequality $-\delta_1\rho(0)<e_{y0}<\delta_2\rho(0)$. The design parameters of the controller and PPF are chosen as $\rho_0=0.09$, $\delta_1=1$, $\delta_2=1$, $r=0.9$, and $\rho_\infty=0.007$. The simulation results are shown in Fig. 14, which indicates that the proposed control method demonstrates better control performance with a smaller steady-state error less than 0.002 p.u. and achieves slightly faster convergence speed compared with the LMPC method without prescribed performance, whose steady-state error is about 0.005 p.u..

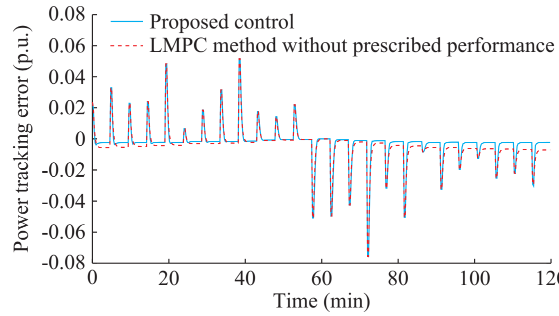

Fig. 14. Power tracking error curve with different control approaches.

V. Conclusion

By introducing indoor mass temperature, the original bilinear aggregate model of TCLs is enhanced by the second-order equivalent thermal parameter model. An LMPC algorithm with prescribed performance is proposed for ATCLs to maintain the power balance between the supply side and demand side. The conclusions are given as follows.

1) The improved bilinear aggregate model optimizes the cumulative error of the innovative model over a long time scale and the dynamic thermal process of ATCLs is described more precisely.

2) The proposed control approach designed in a priori manner improves the control performance both in steady state and transient state, and has a faster convergence speed compared with the algorithm without prescribed performance function.

3) ATCLs can be effectively dispatched by the proposed control method to smooth the power fluctuation of renewable energy without increasing dispatch burden on supply side, and the operating efficiency of the entire system is improved.

Appendix A

The detailed coefficient matrices for the bilinear aggregate model $\boldsymbol{A}$:

$$\boldsymbol{A}=\frac{1}{\Delta T}\begin{bmatrix}\boldsymbol{A}_{11} & \boldsymbol{A}_{12}\\ \boldsymbol{A}_{21} & \boldsymbol{A}_{22}\end{bmatrix} \tag{A1}$$

$$\boldsymbol{A}_{11}=\begin{bmatrix} -\alpha_{off} & & & & \\ \alpha_{off} & -\alpha_{off} & & & \\ & \ddots & \ddots & & \\ & & \alpha_{off} & -\alpha_{off} & \\ & & & \ddots & \ddots \\ & & & \alpha_{off} & -\alpha_{off} \end{bmatrix} \tag{A2}$$

$$\boldsymbol{A}_{22}=\begin{bmatrix} \alpha_{on} & -\alpha_{on} & & & \\ & \ddots & \ddots & & \\ & & \alpha_{on} & -\alpha_{on} & \\ & & & \ddots & \ddots \\ & & & \alpha_{on} & -\alpha_{on} \\ & & & & \alpha_{on} \end{bmatrix} \tag{A3}$$

where $\boldsymbol{A}_{11},\boldsymbol{A}_{22}\in\mathbf{R}^{F\times F}$; $A_{12}(D+1,F+1)=\alpha_{on}$; $A_{21}(G,F)=\alpha_{off}$;

other elements of matrices $\boldsymbol{A}_{12}$, $\boldsymbol{A}_{21}$ are zeros; $F=L/2$; and D and G are the numbers of temperature intervals at the boundary in the finite difference process.

References

[1] S. R. Sinsel, R. L. Riemke, and V. H. Hoffmann, "Challenges and solution technologies for the integration of variable renewable energy sources–a review," *Renewable Energy*, vol. 145, pp. 2271-2285, Jan. 2020.

[2] A. Basit, A. D. Hansen, M. Altin *et al*., "Compensating active power imbalances in power system with large-scale wind power penetration," *Journal of Modern Power Systems and Clean Energy*, vol. 4, no. 2, pp. 229-237, Jul. 2015.

[3] J. Wang, Z. Zhou, J. Zhao *et al*., "Optimizing for clean-heating improvements in a district energy system with high penetration of wind power," *Energy*, vol. 175, pp. 1085-1099, May 2019.

[4] J. A. Pinzon, P. P. Vergara, L. Silva *et al*., "Optimal management of energy consumption and comfort for smart buildings operating in a microgrid," *IEEE Transactions on Smart Grid*, vol. 10, no. 3, pp. 3236-3247, Apr. 2018.

[5] B. Biegel, P. Andersen, J. Stoustrup *et al*., "Sustainable reserve power from demand response and fluctuating production–two Danish demonstrations," *Proceedings of the IEEE*, vol. 104, no. 4, pp. 780-788, Apr. 2016.

[6] J. Hu, J. Cao, M. Chen *et al*., "Load following of multiple heterogeneous TCL aggregators by centralized control," *IEEE Transactions on Power Systems*, vol. 32, no. 4, pp. 3157-3167, Jul. 2017.

[7] J. L. Mathieu, S. Koch, and D. S. Callaway, "State estimation and control of electric loads to manage real-time energy imbalance," *IEEE Transactions on Power Systems*, vol. 28, no. 1, pp. 430-440, Feb. 2013.

[8] N. Lu and D. P. Chassin, "A state-queueing model of thermostatically controlled appliances," *IEEE Transactions on Power Systems*, vol. 19, no. 3, pp. 1666-1673, Aug. 2004.

[9] R. Malhame and C. Y. Chong, "Electric load model synthesis by diffusion approximation of a high-order hybrid-state stochastic system," *IEEE Transactions on Automatic Control*, vol. 30, no. 9, pp. 854-860, Sep. 1985.

[10] S. Bashash and H. K. Fathy, "Modeling and control of aggregate air conditioning loads for robust renewable power management," *IEEE Transactions on Control Systems Technology*, vol. 21, no. 4, pp. 1318-1327, Jul. 2013.

[11] X. Chen, J. Wang, J. Xie *et al*., "Demand response potential evaluation for residential air conditioning loads," *IET Generation, Transmission & Distribution*, vol. 12, no. 19, pp. 4260-4268, Sept. 2018.

[12] L. M. Cheng and Y. Q. Bao, "A day-ahead scheduling of large-scale thermostatically controlled loads model considering second-order equivalent thermal parameters model," *IEEE Access*, vol. 8, pp. 102321-102334, Jun. 2020.

[13] X. Wu, J. He, Y. Xu *et al*., "Hierarchical control of residential HVAC units for primary frequency regulation," *IEEE Transactions on Smart Grid*, vol. 9, no. 4, pp. 3844-3856, Jul. 2018.

[14] P. Bajaria and N. M. Singh, "Dynamic dispatch of thermostatically controlled loads using phase oscillator model," *Sustainable Energy Grids & Networks*, vol. 18, pp. 1-9, Jun. 2019.

[15] W. Zhang, J. Lian, C. Y. Chang *et al*., "Aggregated modeling and control of air conditioning loads for demand response," *IEEE Transactions on Power Systems*, vol. 28, no. 4, pp. 4655-4664, Nov. 2013.

[16] J. Yang, T. Liu, H. Wang *et al*., "Optimizing the regulation of aggregated thermostatically controlled loads by jointly considering consumer comfort and tracking error," *Energies*, vol. 12, no. 9, pp. 1-17, May. 2019.

[17] H. Zhao, Q. Wu, S. Hang *et al*., "Hierarchical control of thermostatically controlled loads for primary frequency support," *IEEE Transactions on Smart Grid*, vol. 9, no. 4, pp. 2986-2998, Jul. 2018.

[18] S. Lin, D. Liu, F. Hu *et al*., "Grouping control strategy for aggregated thermostatically controlled loads," *Electric Power Systems Research*, vol. 171, pp. 97-104, Jun. 2019.

[19] N. Mahdavi, J. H. Braslavsky, M. M. Seron *et al*., "Model predictive control of distributed air-conditioning loads to compensate fluctuations in solar power," *IEEE Transactions on Smart Grid*, vol. 8, no. 6, pp. 3055-3065, Nov. 2017.

[20] C. Lv, H. Yu, P. Li *et al*., "Model predictive control based robust scheduling of community integrated energy system with operational flexibility," *Applied Energy*, vol. 243, pp. 250-265, Jun. 2019.

[21] S. Fan and C. Tong, "Model predictive current control method for PMSM drives based on an improved prediction model," *Journal of Power Electronics*, vol. 20, no. 8, pp. 1456-1466, Aug. 2020.

[22] L. Zhang, S. Xu, X. Ju *et al*., "Flexible satellite control via fixed-time prescribed performance control and fully adaptive component synthesis vibration suppression," *Nonlinear Dynamics*, vol. 100, no. 4, pp. 3413-3432, May 2020.

[23] H. Wu, S. Liu, C. Cheng *et al*., "Observer based adaptive double-layer fuzzy control for nonlinear systems with prescribed performance and unknown control direction," *Fuzzy Sets and Systems*, vol. 392, pp. 93-114, Aug. 2020.

[24] B. Zhang, L. Jiang, and J. Bai, "Velocity-free prescribed performance control for spacecraft hovering over an asteroid with input saturation," *Journal of the Franklin Institute*, vol 357, no. 11, pp. 6471-6497, Jul. 2020.

[25] J. Zhang, S. Wang, P. Zhou *et al*., "Novel prescribed performance-tangent barrier Lyapunov function for neural adaptive control of the chaotic PMSM system by backstepping," *International Journal of Electrical Power & Energy Systems*, vol. 121, pp. 1-12, Oct. 2020.

[26] Y. Huang, J. Na, X. Wu *et al*., "Adaptive control of nonlinear uncertain active suspension systems with prescribed performance," *ISA Transactions*, vol. 54, pp. 145-155, Jan. 2015.

[27] S. Iacovella, F. Ruelens, P. Vingerhoets *et al*., "Cluster control of heterogeneous thermostatically controlled loads using tracer devices," *IEEE Transactions on Smart Grid*, vol. 8, no. 2, pp. 528-536, Mar. 2017.

[28] S. Bashash and H. K. Fathy, "Modeling and control of aggregate air conditioning loads for robust renewable power management," *IEEE Transactions on Control Systems Technology*, vol. 21, no. 4, pp. 1318-1327, Jul. 2013.

[29] M. P. Akter, S. Mekhilef, N. L. Tan *et al*., "Modified model predictive control of a bidirectional AC-DC converter based on lyapunov function for energy storage systems," *IEEE Transactions on Industrial Electronics*, vol. 63, no. 2, pp. 704-715, Feb. 2016.

[30] S. Golzari, F. Rashidi, and H. F. Farahani, "A Lyapunov function based model predictive control for three phase grid connected photovoltaic converters," *Solar Energy*, vol. 181, pp. 222-233, Mar. 2019.

[31] Y. Zhang, C. Hua, and K. Li, "Disturbance observer-based fixed-time prescribed performance tracking control for robotic manipulator," *International Journal of Systems Science*, vol. 50, no. 13, pp. 1-12, Sept. 2019.

[32] X. Wang, X. Yin, Q. Wu *et al*., "Disturbance observer based adaptive neural control of uncertain MIMO nonlinear systems with unmodeled dynamics," *Neurocomputing*, vol. 313, pp. 247-258, Nov. 2018.

[33] Y. Li, S. Tong, L. Liu *et al*., "Adaptive output-feedback control design with prescribed performance for switched nonlinear systems," *Automatica*, vol. 80, pp. 225-231, Jun. 2017.

[34] C. Wang and Z. Zuo, "Adaptive trajectory tracking control of output constrained multi-rotors systems," *IET Control Theory & Applications*, vol. 8, no. 13, pp. 1163-1174, Sept. 2014.

Yang Yu received the M.S. degree in electrical engineering in 2008 from Xi'an Jiaotong University, China, and the Ph.D. degree in electrical engineering in 2016 from North China Electric Power University (NCEPU), Beijing, China. He is currently an Associate Professor at the State Key Laboratory of Alternate Electrical Power System with Renewable Energy Sources, NCEPU, Baoding, China. His research interests include electrical energy storage technology and optimal dispatch of flexible load.

Li Quan received the B.S. degree in electrical engineering in 2018 from Yanshan University, Qinhuangdao, China. She is currently pursuing the M.S. degree at Hebei Key Laboratory of Distributed Energy Storage and Micro-grid, North China Electric Power University (NCEPU), Baoding, China. Her research interests include optimal dispatch and control of flexible load.

Zengqiang Mi received the M.S. degree in electrical engineering in 1986 from North China Electric Power University (NCEPU), Baoding, China. He is currently a Professor at the State Key Laboratory of Alternate Electrical Power System with Renewable Energy Sources, NCEPU, Baoding, China. His research interests include power system operation and control, electrical energy storage technology, and optimal dispatch of flexible load.

Jianbin Lu received the M.S. degree in electrical engineering from North China Electric Power University (NCEPU), Baoding, China, in 2020. He is currently working in the Electric Power Research Institute of Guangxi Pow-

er Grid Co., Ltd., Nanning, China. His research interests include optimal dispatch and control of flexible load.

Shengqiang Chang received the B.S. degree in electronic engineering from Hebei University of Technology, Tianjin, China, in 2001. He is currently a Senior Engineer and Vice President of Research Institute of Shijiazhuang Kelin Electric Co., Ltd., Shijiazhuang, China, and General Manager of Shijiazhuang Kelin Cloud Energy Information Technology Co., Ltd., Shijiazhuang, China. His research interests include power system automation and software products. In recent years, he mainly studies on integrated energy management and control based on Internet-of-Things, big data, and artificial intelligence technology.

Yubao Yuan received the B.S. degree of computer science and technology from North China Electric Power University, Baoding, China, in 2007. He is currently a Senior Engineer of Shijiazhuang Kelin Electric Co., Ltd., Shijiazhuang, China, and Project Manager of Shijiazhuang Kelin Yunneng Information Technology Co., Ltd., Shijiazhuang, China. His research interests include basic software technology, information security and power automation monitoring system.